Colloid Polym Sci (2008) 286:907–916
DOI 10.1007/s00396-008-1846-6

ORIGINAL CONTRIBUTION

Preparation of PMMA/acid-modified chitosan core-shell nanoparticles and their potential as gene carriers

Nuttaporn Pimpha · Uracha Rattanonchai · Suvimol Surassmo · Praneet Opanasopit · Chonticha Rattanarungchai · Panya Sunintaboon

Received: 9 August 2007 / Revised: 31 January 2008 / Accepted: 31 January 2008 / Published online: 9 April 2008

Abstract The core-shell nanoparticles consisting of poly (methyl methacrylate) (PMMA) cores surrounded by various acid-modified chitosan shells were synthesized using a surfactant-free emulsion copolymerization, induced by a *tert*-butylhydroperoxide (TBHP) solution. Methyl methacrylate (MMA) was grafted onto four acid-modified chitosans (hydrochloric, lactic, aspartic, and glutamic acids) with MMA conversions up to 64%. The prepared nanoparticles had diameter ranging from 100 to 300 nm characterized by atomic force microscopy and displayed highly positive surface charges up to +77 mV. Transmission electron microscopic images clearly revealed well-defined core-shell morphology of the nanoparticles where PMMA cores were coated with acid-modified chitosan shells. The effect of acid-modified chitosans on particle size, intensity of surface charge, morphology, and thermal stability were determined systematically. The plasmid DNA/nanoparticles complexes were investigated with ζ-potential measurement. The results suggested that these nanoparticles can effectively complex with plasmid DNAs via electrostatic interaction and could be used as gene carriers.

N. Pimpha · U. Rattanonchai · S. Surassmo
National Nanotechnology Center,
National Science and Technology Development Agency,
Pathumthani 12120, Thailand

P. Opanasopit
Faculty of Pharmacy, Silpakorn University,
Nakhonpathom 73000, Thailand

C. Rattanarungchai · P. Sunintaboon (✉)
Department of Chemistry, Faculty of Science, Mahidol University,
Bangkok 10400, Thailand
e-mail: scpsu@mahidol.ac.th

Keywords Core-shell nanoparticles · Acid-modified chitosan · Poly(methyl methacrylate) (PMMA) · Gene carrier · Surfactant-free

Abbreviations

PMMA	poly(methyl methacrylate)
TBHP	*tert*-butylhydroperoxide
MMA	methyl methacrylate
AFM	atomic force microscopy
TEM	transmission electron microscopy
pDNA	plasmid DNA
HCL	hydrochloric acid
ASP	aspartic acid
GLU	glutamic acid
LAC	lactic acid
DI	deionized
PCS	photon correlation spectroscopy
TGA	thermogravimetric analysis
DSC	differential scanning calorimetry
FTIR	Fourier-transformed infrared spectrophotometry
CH-HCL	hydrochloric acid-modified chitosan
CH-ASP	aspartic acid-modified chitosan
CH-LAC	lactic acid-modified chitosan
CH-GLU	glutamic acid-modified chitosan
ζ-potential	zeta-potential
$-NH_3^+$	aminium ion
PMMA/CH-HCL	poly(methyl methacrylate)/ hydrochloric acid-modified chitosan core-shell nanoparticles
PMMA/CH-ASP	poly(methyl methacrylate)/aspartic acid -modified chitosan core-shell nanoparticles

PMMA/CH-LAC	poly(methyl methacrylate)/lactic acid-modified chitosan core-shell nanoparticles
PMMA/CH-GLU	poly(methyl methacrylate)/glutamic acid-modified chitosan core-shell nanoparticles
ISP	isoelectric point
Tg	glass transition temperature

Introduction

A polymeric colloidal micro- and nanoparticle possessing an extremely large surface area is an attractive candidate as a carrier vehicle for bioactive substances, such as therapeutic drugs, proteins, genes, or enzymes. For such application, colloidal particles prepared from biocompatible and biodegradable polymers are desirable. Chitosan, a β-(1,4)-linked polysaccharide of D-glucosamine, is a deacetylated form of chitin, the second most abundant natural polymer on the planet earth and obtained from shells of lobsters, prawns, and crabs. It has interesting properties, such as biocompatibility, biodegradability, film forming ability, gelation characteristics, and bioadhesion [1–5]. In addition, it has long been used as a biopolymer and a natural material in pharmaceutical and medical applications, food, and wastewater treatment [6–18]. Because of its polycationic nature, chitosan has been extensively investigated for carrier and delivery systems of negatively charged agents. Chitosan can effectively bind to DNAs and protect them from nuclease degradation because positively charged chitosan can be easily complexed with negatively charged DNAs [19–21]. Furthermore, there are evidences demonstrating that chitosan, a cationic polymer, plays an important role in both membrane adhesion and lysosomal escape of the encapsulated DNA [22–24].

To prepare positively charged chitosan nanoparticles, emulsion polymerization of vinyl monomers onto chitosan is widely used [25–28]. For example, hydroxyl groups on chitosan are capable of acting as a nucleophilic agent to initiate the polymerization of methyl methacrylate (MMA). Chauvierre et al. [25] reported the preparation of chitosan-decorated poly(isobutyl cyanoacrylate) by the dextran-cerium (IV) redox system under an acidic aqueous condition. Hsu et. al. also mentioned the synthesis of chitosan-modified poly (methyl methacrylate) (PMMA) by emulsion polymerization with potassium persulfate as an initiator [26]. Recently, Ye et al. [27] reported the new facile route to chitosan nanoparticles by an emulsifier-free emulsion copolymerization of MMA in free-radical initiation from amine groups of chitosan. Ye et al. [28] developed the chitosan core-shell nanoparticles with poly(butyl acrylate) core for textile coatings. Unfortunately, chitosan used in the above methods was dissolved in an excessively acidic aqueous solution, which was not suitable for medical application. An excess acid is not desirable and very detrimental to acid-labile bioactive substances. Therefore, there were many attempts to develop chitosan salts with various acids to reduce the excessive acids and its fatality. Chitosan derivatives from glutamate, aspartate, and hydrochloride salts were reported to be used in drug delivery specifically to colon [29]. In addition, they can be used to enhance the peptide delivery across intestinal epithelia [30]. Herein, we report the preparation and characterization of chitosan nanoparticles using the chitosans modified with hydrochloric, lactic, glutamic, and aspartic acids by the emulsifier-free emulsion polymerization. Their potential as gene carriers is also included.

Materials and methods

Materials

Chitosan was purchased from Seafresh Chitosan Lab., Thailand. The degree of deacetylation was about 85%, and average molecular weight of chitosan was about 45 kDa, determined by a viscometric method. Glutamic acid, aspartic acid, and lactic acid were purchased from Ajax Finechem. MMA and *t*-butyl hydroperoxide (TBHP) were purchased from Fluka. TBHP was used without further treatment. MMA was purified using a column packed with alumina adsorbent. Deionized (DI) and autoclaved water were sterilized and used throughout the study. All other chemicals were commercially available and of analytical grade.

Preparation of acid-modified chitosans

Chitosan salts were prepared by a freeze-drying technique. Briefly, chitosan powder was completely dissolved in DI water containing hydrochloric acid (HCL), aspartic acid (ASP), glutamic acid (GLU), and lactic acid (LAC). The average molar ratio of glucosamine units in chitosan to each acid was 1:0.80. A weight of the solution was adjusted with DI water to make 1% *w*/*w* solution and stirred for 12 h. The final pH of each acid-modified chitosan solution was in a range of 4–6. This solution was filtered and freeze-dried (Cryodos, Telstar, New Zealand). The dried powder obtained was collected and stored in a desiccator containing dry silica gel before use in each experiment.

Preparation of chitosan core-shell nanoparticles

An emulsifier-free emulsion polymerization was conducted by using a redox-initiating system consisting of amine

groups from the chitosan backbone and TBHP. A batch process of emulsifier-free emulsion polymerization was conducted in a 100-ml water-jacketed glass reactor equipped with nitrogen inlet, reflux condenser, water cooling system, and magnetic stirrer. A predissolved acid-modified chitosan (0.5 g), including purified MMA monomer (1 g) and water (47.5 g), were charged to the reactor and were degassed with N_2 gas for 30 min under 500 rpm stirring rate. Water was pumped through the jacketed reactor from a thermostat water bath, which was controlled at 80±1 °C. Then, the TBHP aqueous solution (1 g, 5×10^{-3} M) was added to the reaction mixture to start polymerization. The nitrogen gas was bubbled throughout the course of polymerization. Operation conditions were similar for all polymerizations conducted in this work. The resulted particles were purified by centrifugation at 10,000 rpm for 1 h for two to three times to remove unreacted starting materials.

Determination of monomer conversion

Monomer conversions were determined gravimetrically. About 2 g of latex was taken to a preweighed aluminum disposable pan after each polymerization was terminated. After letting all volatile components to evaporate in fume-hood, samples were then dried in a vacuum oven until their weight remained unchanged at 70 °C. Monomer conversions were calculated from the weights of monomers charged and those of dried polymers obtained from a taken latex.

$$\%\text{conversion} = \frac{\text{weight of dried latex} - \text{weight of chitosan}}{\text{weight of monomer feed}} \times 100$$

$$\%\text{solids content} = \frac{\text{weight of dried latex}}{\text{weight of latex}} \times 100$$

By assuming that the weight fraction of chitosan in a batch reactor before starting polymerization is the same as that in latex after polymerization, the weight of chitosan in the equation above can be calculated with the same proportion at any amount of latex taken [31].

Morphological characterization

Morphology of the chitosan core-shell nanoparticles and size were observed with an atomic force microscope (AFM, Seiko, Japan). A diluted chitosan nanoparticle latex was deposited onto a freshly cleaved mica substrate. A sample was imaged after water evaporation. An experiment was performed with a tapping mode using NSG 10 cantilever with 190–325 kHz resonance frequency. All images were recorded in air at room temperature at a scan speed of 1 Hz. A transmission electron microscope (TEM; Tecnai G2 Sphera, at an accelerating voltage of 80 kV) was also utilized to observe the morphology and size of the particles. A drop of latex sample diluted with DI water was dried on a formva-coated copper grid. Then, the sample was stained with 2% phosphotungstic acid aqueous solution for 3 min before analyzed.

Particle size of chitosan core-shell nanoparticles

Measurement of hydrodynamic diameter and polydispersity index (PDI) of nanoparticles were performed using photon correlation spectroscopy (PCS; NanoZS 4700, Malvern Instruments, UK). All formulations (10 μl) were diluted with 1 ml of filtered deionized water to eliminate the effect of viscosity caused by ingredients. Polydispersity indexes were measured from the size distribution of nanoparticle population. Each value reported was an average of at least three measurements.

ζ-Potential of chitosan core-shell nanoparticles

A magnitude of electrostatic charges of nanoparticle surface was determined by measuring ζ-potential of nanoparticle dispersion. ζ-Potential values were obtained by using zetasizer (NanoZS 4700, Malvern Instruments) in 1 mM NaCl solution at room temperature. All measurements were done at a wavelength of 633 nm at 25 °C with a scattering angle of 90°. The results reported were the mean of three determinations.

FTIR analysis

Infrared spectra were obtained using an EQUINOX55 FT-IR spectrophotometer combined to PC with OPUS analysis software. The grafted products were previously dried to be a powder and then placed on an ATR crystal for a pass of single reflection with a laser beam. The spectra were recorded at a resolution of 4 cm^{-1} and 32 scans.

Thermal properties

Thermogravimetric analysis was conducted to study the thermal stability of chitosan, chitosan salts, and nanoparticles of chitosan salts. TGA thermograms were obtained using a thermogravimetric analyzer (TGA/SDTA851, Mettler, Switzerland). The sample of 5–10 mg was accurately weighed in an aluminum pan. The measurement was conducted at a heating rate of 10 °C/min under a nitrogen purge.

Tgs of the particles were determined by using a differential scanning calorimeter (DSC823e/700, Mettler). The instrument was calibrated with an Indium standard and a nitrogen atmosphere (flow rate=50 ml/min) was used

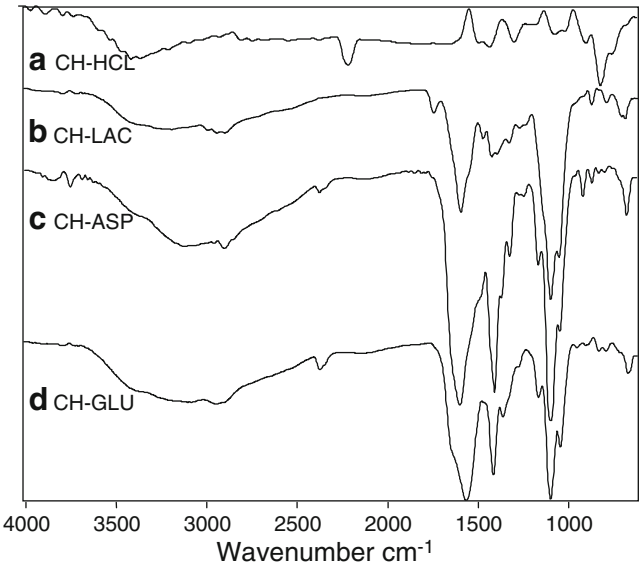

Fig. 1 FT-IR spectra of chitosan hydrochloride (*CH-HCL*), chitosan lactate (*CH-LAC*), chitosan aspartate (*CH-ASP*), and chitosan glutamate (*CH-GLU*) prepared by freeze-drying

throughout. Heating was carried out at 10 °C/min in the temperature range of 0 to 300 °C.

The chitosan nanoparticle–pDNA complex formation

Different amounts of the nanoparticle dispersion were mixed with 2.2 mg/ml of the plasmid DNAs (pDNAs) containing pSV-β-galactosidase as a reporter gene in DI water. The mixtures were then incubated at room temperature for 15 min to ensure a complex formation. The binding efficiency was then analyzed.

Results and discussion

Characterization of the acid-modified chitosans

Fourier-transformed infrared spectrophotometry (FTIR) measurements were performed to analyze the functional group composition of the acid-modified chitosans: chitosan hydrochloride (CH-HCL), chitosan lactate (CH-LAC), chitosan aspatate (CH-ASP), and chitosan glutamate (CH-GLU). The FTIR spectra of CH-GLU, CH-LAC, and CH-ASP showed strong asymmetric and symmetric carboxylate anion stretching peaks in a range of 1,546–1,548 and 1,389–1,400 cm^{-1} indicating the presence of carboxylic groups from those acids in the molecular structure of the chitosans as shown in Fig. 1. However, these peaks did not appear in CH-HCL due to the absence of carboxylic group in the hydrochloric salt. The peaks in a range of 1,069–1,091 cm^{-1} corresponded to the aminium ion ($-NH_3^+$) rocking of chitosan. Therefore, these results indicated that the chitosans modified with the four acids can be obtained.

Preparation of chitosan core-shell nanoparticles

Next, the core-shell nanoparticles were synthesized. Such particles were designed to have the chitosans, modified with the four acids described in the previous section, on their surfaces. PMMA was a core component that acts as a neutral solid support for the particles with a good mechanical strength. These particles were synthesized using an emulsifier-free emulsion copolymerization by the method reported by Li et al. [31]. Copolymerization of MMA from the water-soluble acid-modified chitosan (MMA: chitosan=2:1 by weight) can be triggered by the small amount of TBHP (5×10^{-3} M). Each reaction was conducted at 80 °C for 2 h. In this polymerization, both amphiphilic-grafted copolymer of PMMA and chitosan and homo-PMMA can be formed simultaneously. Core-shell particles could be obtained from the following plausible mechanism. Once the amphiphilic-grafted copolymers were formed, they phase separated by aggregating as micelle-like microdomains or precipitating on themselves, which could be called primary particles. These primary particles could be sites for further polymerization of MMA leading to the growth of polymer particles, entrapping homo-PMMA inside due to a hydrophobic preference between homo-PMMA and the grafted PMMA on chitosan [31, 32]. Finally, PMMA/acid-modified chitosan core-shell particles, PMMA/CH-HCL, PMMA/CH-LAC, PMMA/CH-ASP, and PMMA/CH-GLU, can be formed. Monomer conversion and solids content of the core-shell nanoparticles prepared from the acid-modified chitosans are shown in Table 1.

From our preliminary investigation, we found that the weight ratio of chitosan salts to MMA of 0.5:1 g was suitable for the formation of stable core-shell nanoparticles. If the amount of MMA used was higher, white chunky precipitation was formed at an early stage of polymerization. However, at the lower amount of MMA, the latexes

Table 1 Monomer conversion and solids content of core-shell nanoparticles

Particles	% Conversion	% Solids content
PMMA/CH-HCL	55±8	2.2±0.4
PMMA/CH-LAC	64±2	2.3±0.1
PMMA/CH-ASP	63±3	2.3±0.1
PMMA/CH-GLU	56±1	2.1±0.1

PMMA/CH-HCL particles from hydrochloric acid-modified chitosan, *PMMA/CH-LAC* particles from lactic acid-modified chitosan, *PMMA/CH-ASP* particles from aspartic acid-modified chitosan, *PMMA/CH-GLU* particles from glutamic acid-modified chitosan

obtained were quite dilute. Therefore, at the specific ratio (0.5:1 g chitosan/MMA or 1:2 by weight), the core-shell nanoparticles can be resulted with monomer conversions of 55–64%. In fact, the monomer conversions obtained at this condition were quite low. This may be due to the less active aminium groups to generate free radicals after forming redox pairs with the TBHP. These results corresponded well with the previous report showing that primary amino groups are the most effective groups for generating free radicals compared to the secondary, tertiary, or even quaternary ones [32]. Although there are a large number of primary amino groups on the chitosan used (85% degree of deacetylation), most of them were transformed to aminium salts with the acids. This resulted in the fewer amounts of the most reactive primary amino groups and a large amount of less reactive aminium groups, leading to low monomer conversions at the condition conducted.

Size and size distribution of chitosan core-shell nanoparticles

The size and size distribution of the PMMA-chitosan nanoparticles were determined using the PCS analysis and AFM as shown in Table 2. The PMMA/CH-HCL nanoparticles had the average diameter of 376 nm, while PMMA/CH-LAC, PMMA/CH-ASP, and PMMA/CH-GLU nanoparticles exhibited larger particle sizes of 471, 657, and 765 nm, respectively. All particles obtained had the polydispersity index in a range of 0.13–0.22 indicating a narrow size distribution.

The result from AFM images indicated that the average particle diameters of PMMA/CH-HCL, PMMA/CH-LAC, PMMA/CH-ASP, and PMMA/CH-GLU were 122, 127, 180, and 232 nm, respectively, as also shown in Table 2.

The difference in size of the particles observed by PCS and AFM is reasonable. The particle size determined by PCS was based on the intensity of scattered light and measurement of the movement of particles undergoing Brownian motion. In the solution, the chitosan shell highly swelled due to the expansion of charged groups, both aminium groups on the backbone and the intact counter groups (aspartate and glutamate), on the particle surface. In addition, there would be some possible aggregation of the particles, especially in the case of aspartate or glutamate counter groups, because of their amphoteric property. For these reasons, particle sizes measured by PCS tended to be larger. In AFM, a thin film of polymer latex was scanned at dry state, the expansion of the chitosan shell was limited. Therefore, the sizes determined by this method were smaller. Moreover, the approach of AFM tip to the particle surface could also affect the size determined. However, the particle sizes measured from the two methods were in similar order. The particle sizes were increasing in the following order: PMMA/CH-HCL < PMMA/CH-LAC < PMMA/CH-ASP < PMMA/CH-GLU. The difference in size strongly depended on the acids used to form salts with chitosan. From Scheme 1, in which the chemical structures of the acids were displayed, it can be seen that when those acids form salts with chitosan, they will be automatically attached to the particle surfaces. By that way, these acids would affect the size and stability of the particles. The size of the acids increasing in the order of hydrochloric, lactic, aspartic, and glutamic acids, affects the size of their corresponding particles in the same order (PMMA/CH-HCL < PMMA/CH-LAC < PMMA/CH-ASP < PMMA/CH-GLU). Therefore, this result showed that the particle size and size distribution were dramatically affected by a type of modified chitosan salts.

Surface charge measurement

The surface charge of acid-modified chitosan nanoparticles was studied through a zeta-potential measurement as a function of pHs. The obtained nanoparticles were incubated at different pH values (3.8, 4.6, 5.6, 6.5, 7.1, 9.2, 10.0, and 11.2) in 1 mM NaCl solution at 25 °C, and the result is shown in Fig. 2. At lower pHs, the surface charges of the nanoparticles were positive because the $–NH_3^+$ groups on the chitosan backbone that were already protonated from the acids (hydrochloric, lactic, aspartic, and glutamic acids). The positive zeta-potentials of the nanoparticles at lower pHs [lower than pHs at isoelectric points (ISPs)] indicated that these nanoparticles could have high stability through an electrostatic repulsion in an aqueous medium and high capability of condensing negatively charged pDNAs. However, the highest zeta-potentials of those four

Table 2 Particle size and size distribution of PMMA/acid-modified chitosan nanoparticles determined by PCS and AFM

Nanoparticles	PCS		AFM
	Mean particle diameter (nm)	Polydispersity index	Mean particle diameter (nm)
PMMA/CH-HCL	376.3±0.6	0.13±0.01	122.3±16.2
PMMA/CH-LAC	471.3±8.5	0.13±0.03	127.9±15.6
PMMA/CH-ASP	657.3±14.6	0.14±0.05	180.7±21.3
PMMA/CH-GLU	765.0±9.9	0.22±0.01	232.6±39.8

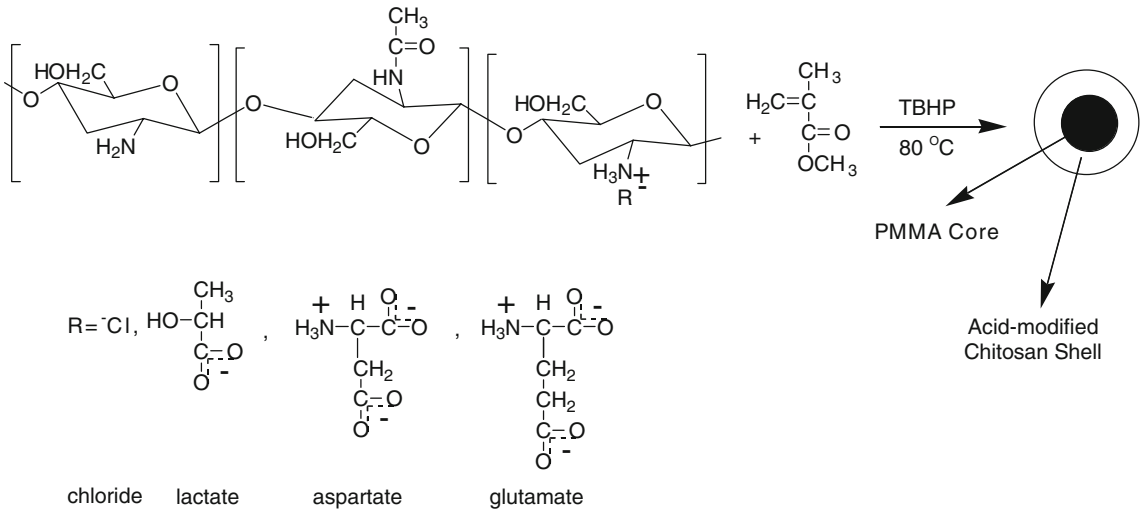

Scheme 1 The preparation of PMMA/acid-modified chitosan nanoparticles by free radical polymerization

types of particles upon changing pH values were varied with the type of complexing acids as concluded in Table 3. Upon increasing pHs, the magnitudes of zeta-potential were less positive, became zero at the ISP and negative beyond the ISPs. This occurred because the cationic $-NH_3^+$ groups were converted back to $-NH_2$ groups. When the basicity increased, the particle surface adsorbed more and more hydroxyl ions from the solution resulting in a negative surface and a negative zeta-potential. From the plot in Fig. 2 and Table 3, the ISPs, which are the pH values at zero surface charge, were given. The ISPs of PMMA/CH-HCL, PMMA/CH-LAC, PMMA/CH-ASP, and PMMA/CH-GLU were at pHs of 8.5, 9.0, 8.3, and 7.2, respectively. This result revealed that the PMMA/CH-LAC particles would be the most stable upon acidity change, while the PMMA/CH-GLU particles were the most susceptible, although they had highest zeta-potential up to +77 mV at pH 4.2.

Moreover, it can be observed that when pH values of the dispersion were higher than 7.0, the particles became unstable, and the significant aggregation was observed when a pH was above 11. This could be explained that, at higher pHs, the modified chitosans on the particle surface are less soluble in water rendering the nanoparticles to aggregate due to the less dipersability in the aqueous medium. Moreover, the low positive surface charge density or even the negative surface charge at higher pHs could not maintain the particle stability.

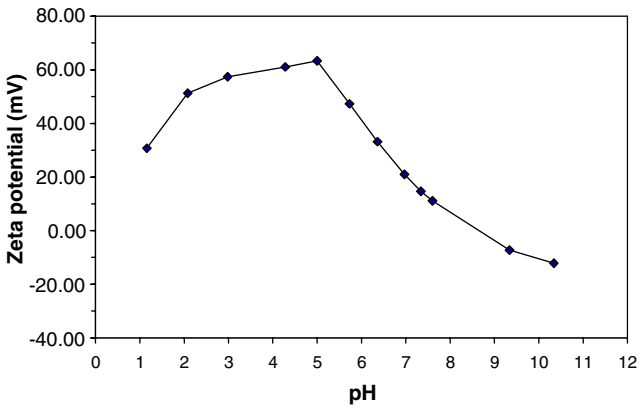

Fig. 2 The effect of pH on zeta potential of PMMA/CH-HCL core-shell nanoparticles

Morphology of chitosan core-shell nanoparticles

AFM is an effective method for providing the exact information about particle size and shape. The AFM image of the core-shell nanoparticles is shown in Fig. 3. It was observed that nanoparticles formed possessed spherical shape.

To determine the core-shell structure, TEM measurement was conducted. With careful staining of the particles using 2% phosphotungstic acid, the core-shell nanostructure of the particles was clearly revealed where the PMMA cores were coated with the chitosan shells. The TEM micrographs of the PMMA/modified chitosan nanoparticles further confirmed that the nanoparticles were spherical (Fig. 4). A stained ring structure was a clear evidence to illustrate the existence of the chitosan on the particle surface because phosphotungstic acid can preferentially react with amine groups of the chitosans.

From the image analysis of TEM micrographs, the particle size and the shell thickness of the particles were concluded in

Table 3 Zeta-potentials of various PMMA/acid-modified chitosan nanoparticles

Particles	Max ζ-potential (mV)	pH at Max ζ-potential	pH at ISP (at 0 mV)
PMMA/CH-HCL	+68	5.1	8.5
PMMA/CH-LAC	+67	3.5	9.0
PMMA/CH-ASP	+68	5.0	8.3
PMMA/CH-GLU	+77	4.2	7.2

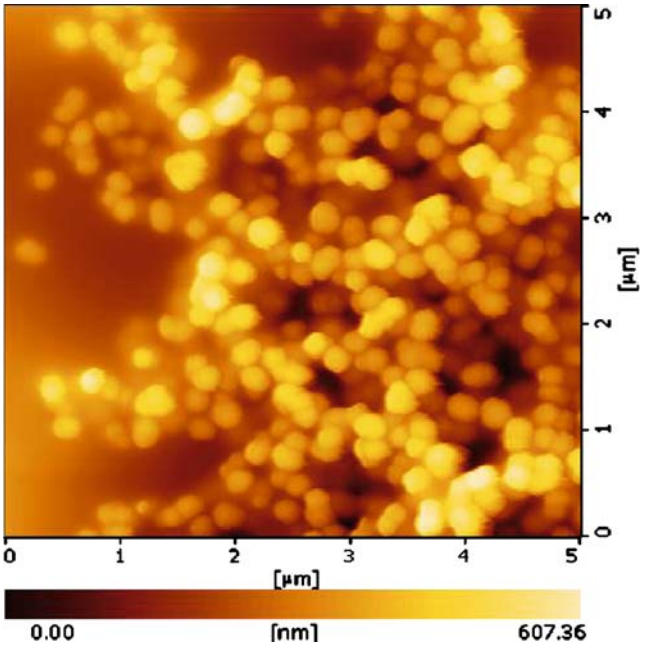

Fig. 3 AFM photographs of PMMA/CH-GLU core-shell nanoparticles

Table 4. We found that the order of the size was in accordance with the previous two methods (PCS and AFM): PMMA/CH-HCL < PMMA/CH-LAC < PMMA/CH-ASP < PMMA/CH-GLU, although the values were different. In addition, TEM also provided the information of the shell thickness of the particles, and the result is shown in Table 4.

Thermal properties of the acid-modified chitosan salts and nanoparticles

Thermal degradation behavior of the chitosan powders exhibited a broad three-stage degradation process. The degradation process consisted of the dehydration, deacetylation, and chain scission in the last stage. It was found that the CH-HCL salt provided three-stage degradation similar to the unmodified chitosan. However, the CH-ASP, CH-LAC, and CH-GLU exhibited similar degradation behavior (a three-stage process and data not shown) with one additional stage in the deacetylation range compared to the unmodified chitosan and the CH-HCL salt. However, the thermal degradation of the nanoparticles exhibited four stages. The first-stage degradation was attributed to a loss of water due to an amidation from carboxylate groups in PMMA with associated positive-charged amino groups in chitosan. Both deacetylation and dehydration of chitosan as well as decarboxylation of PMMA chains caused the second- and third-stage degradation. The last stage degradation behavior was mainly due to the chain scission in both PMMA and chitosan.

The glass transition temperature (Tg) of the nanoparticles was measured by a differential scanning calorimetry (DSC). The values were taken from the second run after heating the sample at a rate of 20 °C/min from room temperature to 200 °C and cooling at the same rate. The appearance of a single Tg for each type of nanoparticles

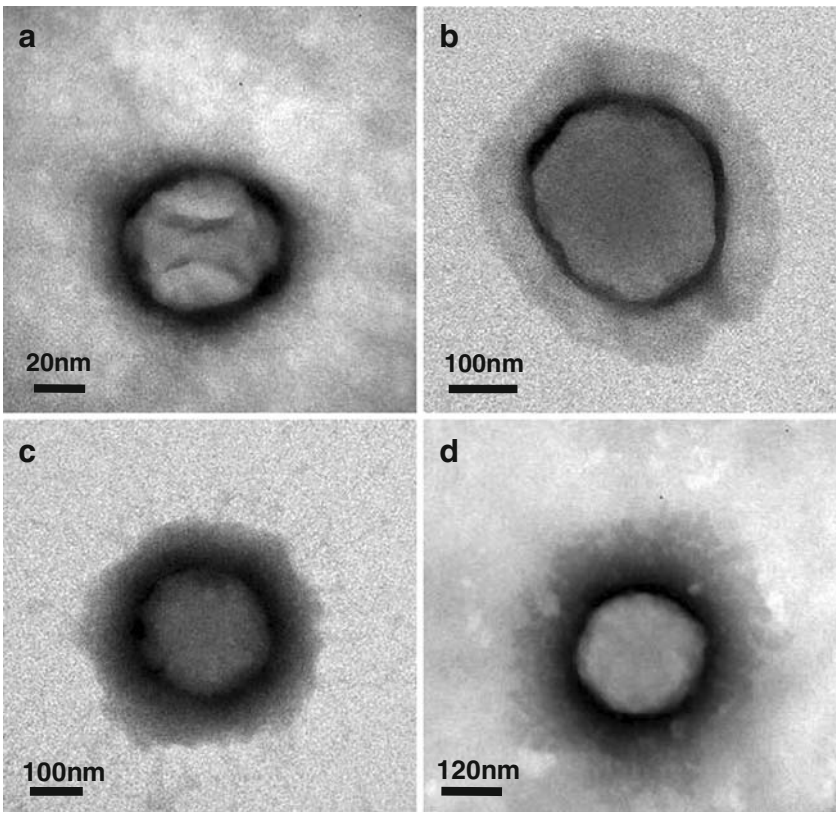

Fig. 4 TEM photographs of PMMA/modified chitosan core-shell nanoparticles: **a** PMMA/CH-HCL, **b** PMMA/CH-LAC, **c** PMMA/CH-ASP, **d** PMMA/CH-GLU

Table 4 The size and the shell thickness of PMMA/acid-modified chitosan nanoparticles determined by TEM

Sample	Size (nm)	Shell thickness(nm)
PMMA/CH-HCL	193±9	36±9
PMMA/CH-LAC	389±32	78±4
PMMA/CH-ASP	414±19	57±19
PMMA/CH-GLU	480±16	90±17

confirmed the formation of graft copolymer between chitosan and MMA, whereas a pure chitosan showed only a broad endothermic peak at low temperature. PMMA/CH-GLU nanoparticles exhibited the highest Tg at 122 °C, while PMMA/CH-ASP, PMMA/CH-LAC, and PMMA/CH-HCL nanoparticles gave Tgs at 119, 115, and 114 °C, respectively.

FTIR analysis of the chitosan core-shell nanoparticles

The grafting of PMMA onto the modified chitosans was confirmed by the FTIR analysis. The spectrum of chitosan was compared with those of the grafted products as shown in Fig. 5. The spectrum of 85% deacethylation chitosan showed the characteristic peaks of amide I (C=O stretching) at 1,648 cm^{-1} and amide II (N–H deformation in plane) at 1,600 cm^{-1} due to the remaining acetamide group in chitosan [33]. The broad peak appeared in a range of 3,205–3,512 cm^{-1} corresponding to O–H stretching at 3,439 cm^{-1} and N–H stretching at 3,366 cm^{-1}. The peaks at 2,892 and 1,384 cm^{-1} were assigned to C–H stretching and $–CH_3$ symmetric deformation, respectively. The strong peak at 1,075 cm^{-1} corresponded to a C–O stretching in ether groups. The grafted products exhibited similar signals to the pure chitosan, except the additional signals at 1,730 cm^{-1} assigned to C=O stretching that belongs to the attached PMMA. In case of PMMA/CH-HCL and PMMA/CH-GLU, the signals belonging to amides I and II cannot be observed. This was probably due to the low relative amount of actual acid-modified chitosans compared to the PMMA in the particles. We tried to prove this by running a new experiment, with a higher amount of the acid-modified chitosan (increasing from 0.5 to 1 g) with the same amount of MMA monomer (1 g). After drying the stable-resulted particles, we can observe those amide signals through an FTIR analysis. However, the FTIR data strongly confirmed the actual occurrence of grafting reaction of PMMA on the chitosan salts.

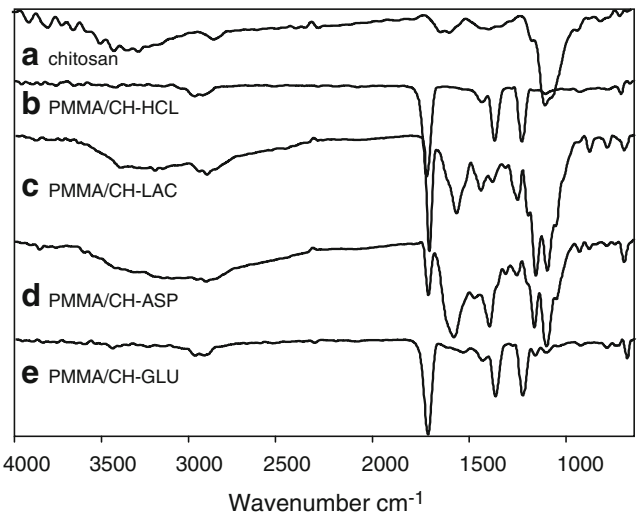

Fig. 5 FT-IR spectra of chitosan and PMMA/modified chitosan core-shell nanoparticles: **a** Chitosan, **b** PMMA/CH-HCL, **c** PMMA/CH-LAC, **d** PMMA/CH-ASP, and **e** PMMA/CH-GLU

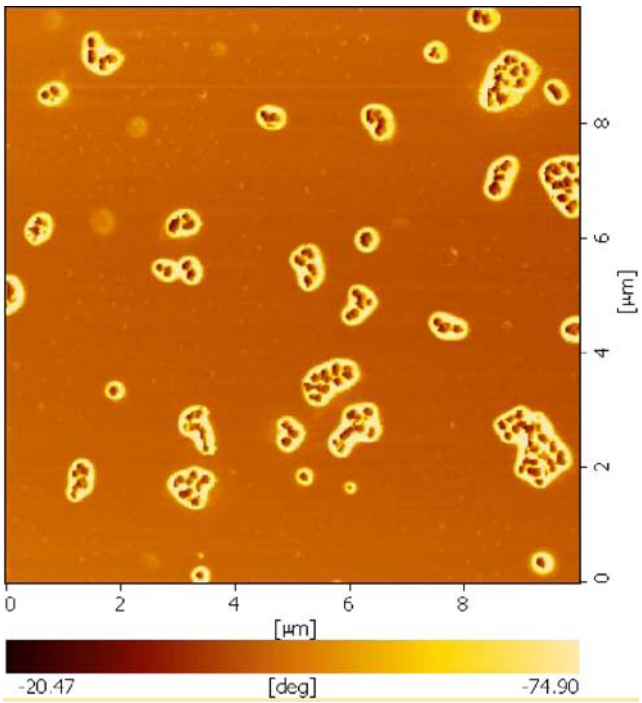

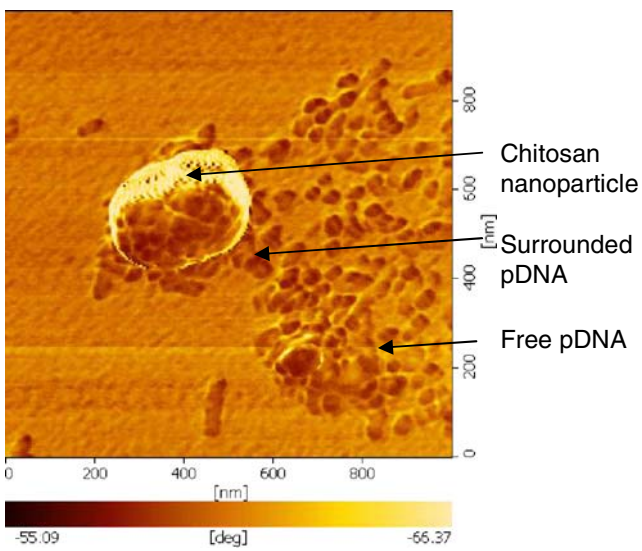

Fig. 6 Phase contrast AFM image of PMMA/CH-ASP core-shell nanoparticles

Determination of particle diameter of chitosan–DNA nanoparticle complexes

The pDNAs were complexed with the chitosan nanoparticles via an electrostatic interaction between amino groups of the nanoparticles and phosphate groups of pDNAs. The change in surface morphologies of chitosan nanoparticles after binding was observed. The AFM image (Fig. 6) displays morphology of the complex. For the phase contrast image analysis, it was obviously found that the chitosan nanoparticles were surrounded by pDNAs.

In this experiment, the mixing ratios were varied with the increasing amount of the nanoparticles, while the amounts of pDNAs were kept constant. It was found that an increase in nanoparticle-to-pDNA ratios resulted in a decrease in particle diameters until reaching a minimum value. The result in Fig. 7 shows the minimum sizes of the complexes of 232, 240, 338, and 254 nm with the ratios 30:1, 25:1 to 30:1, 45:1, and 35:1 for PMMA/CH-HCL, PMMA/CH-LAC, PMMA/CH-ASP, and PMMA/CH-GLU nanoparticles, respectively. A further increase of the nanoparticles resulted in an increase in particle diameters. The reduction of particle sizes was due to the negatively charged pDNA partially neutralizing the positively charged chitosan shell. The chitosan shell therefore became shrunk dimensionally. With a further increase of nanoparticle-to-pDNA ratio, the nanoparticles became unstable and tended to aggregate resulting in an increase of particle size.

In addition, it can be seen that the PMMA/CH-LAC nanoparticles can complex with pDNAs with the least amount compared to other types of nanoparticles indicating that PMMA/CH-LAC nanoparticles have the highest loading capacity. This observation was corresponding well with the information of surface charge neutralization upon changing of pHs previously shown in Table 3. PMMA/CH-LAC nanoparticles had the highest ISP (at pH 9.0). It means that PMMA/CH-LAC nanoparticles could carry more positive charges on their surfaces before being neutralized. Similarly, PMMA/CH-LAC nanoparticles could bind to more negatively charged pDNAs compared

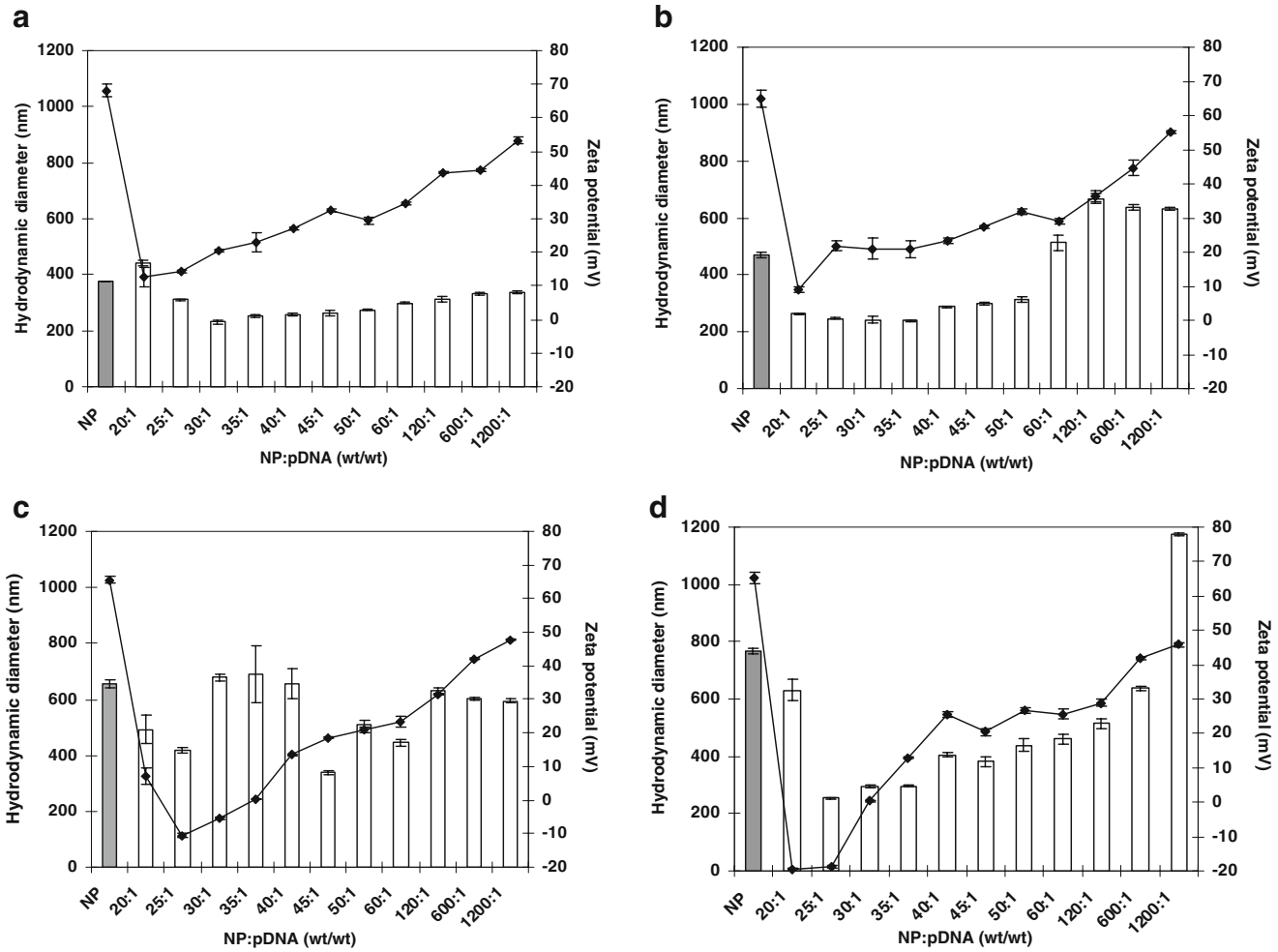

Fig. 7 Particle diameter and size distribution of complexes between PMMA/modified chitosan nanoparticles and DNA: **a** PMMA/CH-HCL, **b** PMMA/CH-LAC, **c** PMMA/CH-ASP, and **d** PMMA/CH-GLU

to other types of the chitosan nanoparticles. Therefore, the pDNA loading capacity of the nanoparticles can be related to the ISPs of the nanoparticles. However, when comparing between PMMA/CH-ASP and PMMA/CH-GLU nanoparticles, it was found that the PMMA/CH-ASP nanoparticles had lower loading capacity, although they had a higher ISP. The higher loading capacity of PMMA/CH-GLU nanoparticles compared to the PMMA/CH-ASP might be due to the non-specific interaction of pDNAs with the larger shell thickness of the PMMA/CH-GLU.

It can be seen that these nanoparticles obviously exhibited a strong binding affinity to pDNAs, which could be possibly used as carriers for gene delivery application. However, a non-biodegradability of PMMA and size of the particles (>200 nm) are also of great concern for their applicability in vivo (intravenous injection possible). Hashida et al. reported that PMMA having molecular weight in a range of 5–40 kDa with positive charges can pass through renal clearance [34]. Therefore, in the next stage of our development, it would be worth to apply our synthetic method to achieve nanoparticles with biodegradable cores and the size below 200 nm. Moreover, information on physico-chemical and pharmacokinetics of nanoparticles in vivo, such as transfection ability, stealt properties, or stability in a biological environment etc., is necessary to be determined.

Conclusions

Chitosan-based core-shell nanoparticles with acid-modified chitosan salts as a shell and PMMA as a core have successfully been synthesized. Size of the prepared nanoparticles was measured by AFM, Zetasizer, and TEM. Although the sizes from three methods were different, they provided the similar relation between particle size in the following order: PMMA/CH-HCL < PMMA/CH-LAC < PMMA/CH-ASP < PMMA/CH-GLU, which increased with the molecular size of acids used to form chitosan salts. TEM clearly demonstrated core-shell morphology of the particles. The shell thickness of particles was also affected by acid-modified chitosan salts. Grafting reaction between PMMA on the chitosan salts was confirmed by FTIR, TGA, and DSC. The high positive zeta-potential indicated that these nanoparticles could have a high stability through an electrostatic repulsion in an aqueous medium. The chitosan nanoparticles can condense with pDNAs via an electrostatic interaction at appropriate ratios, and PMMA/CH-LAC exhibited the highest binding capacity Thus, the investigated core-shell nanoparticles demonstrates their potential as new carriers for DNA delivery.

Acknowledgments The authors are grateful for research funding by the National Nanotechnology Center (Project code NN-B-22-m37-94-49-54) and the Thailand Research Fund, TRF (MRG4880124).

References

1. Ravi Kumar MNV, Muzzarelli RAA, Muzzarelli C, Sashiwa H, Domb AJ (2004) Chem Rev 104:6017
2. Zhao Q, Han B, Wang Z, Gao C, Peng C, Shen J (2007) Nanomed Nanotechnol Biol Med 3:63
3. Rokhade AP, Shelke NB, Patil SA, Aminabhavi TM (2007) Carbohydr Polym 69:678
4. Chen F, Zhang Z-R, Huang Y (2007) Int J Pharm 336:166
5. Bravo-Osuna I, Vauthier C, Farabollini A, Palmieri GF, Ponchel G (2007) Biomaterials 28:2233
6. Zhang C, Ding Y, Yu L, Ping Q (2007) Colloids Surf B Biointerfaces 55:192
7. Yang Y, Chen J, Li H, Wang Y, Xie Z, Wu M, Zhang H, Zhao Z, Chen Q, Fu M, Wu K, Chi C, Wang H, Gao R (2007) Comp Immunol Microbiol Infect Dis 30:19
8. Wang Y-S, Liu L-R, Jiang Q, Zhang Q-Q (2007) Eur Polym J 43:43
9. Lei Z, Bi S, Yang H (2007) Food Chem 104:577
10. Diebold Y, Jarrin M, Saez V, Carvalho ELS, Orea M, Calonge M, Seijo B, Alonso MJ (2007) Biomaterials 28:1553
11. Shi Z, Neoh KG, Kang ET, Wang W (2006) Biomaterials 27:2440
12. Park JS, Han TH, Lee KY, Han SS, Hwang JJ, Moon DH, Kim SY, Cho YW (2006) J Control Release 115:37
13. Maestrelli F, Garcia-Fuentes M, Mura P, Alonso MJ (2006) Eur J Pharm Biopharm 63:79
14. Hyung Park J, Kwon S, Lee M, Chung H, Kim J-H, Kim Y-S, Park R-W, Kim I-S, Bong Seo S, Kwon IC, Young Jeong S (2006) Biomaterials 27:119
15. Chen L, Subirade M (2005) Biomaterials 26:6041
16. Aktas Y, Andrieux K, Alonso MJ, Calvo P, Gursoy RN, Couvreur P, Capan Y (2005) Int J Pharm 298:378
17. Xu Y, Du Y, Huang R, Gao L (2003) Biomaterials 24:5015
18. Janes KA, Fresneau MP, Marazuela A, Fabra A, Alonso MJ (2001) J Control Release 73:255
19. Sang Yoo H, Eun Lee J, Chung H, Chan Kwon I, Young Jeong S (2005) J Control Release 103:235
20. Gan Q, Wang T, Cochrane C, McCarron P (2005) Colloids Surf B Biointerfaces 44:65
21. Chae SY, Son S, Lee M, Jang M-K, Nah J-W (2005) J Control Release 109:330
22. Kiang T, Wen J, Lim HW, Leong KW (2004) Biomaterials 25:5293
23. Takeuchi H, Yamamoto H, Kawashima Y (2001) Adv Drug Deliv Rev 47:39
24. Mao H-Q, Roy K, Troung-Le VL, Janes KA, Lin KY, Wang Y, August JT, Leong KW (2001) J Control Release 70:399
25. Chauvierre C, Labarre D, Couvreur P, Vauthier C (2003) Pharm Res 5:365
26. Hsu S-C Don T-M, Chiu W-Y (2002) J App Polym Sci 86:3047
27. Ye W, Xin JH, Li P, Lee K-LD, Kwong T-L (2006) J App Polym Sci 102:1787
28. Ye W, Leung MF, Xin J, Kwong T-L, Lee K-JD, Li P (2005) Polymer 46:10538
29. Nunthanid JL, Sriamornsak P, Limmatvapirat S, Puttipipatkhachorn S, Lim LY, Khor E (2004) J Control Release 99:15
30. De Campos A, Sanchez A, Alonso MJ (2001) Int J Pharm 224:159
31. Li P, Zhu J, Sunintaboon P, Harris FW (2002) Langmiur 18:8641
32. Li P, Zhu J, Sunintaboon P, Harris FW (2003) J Disp Sci Tech 24:607
33. Amaral FGPL, Barbosa MA (2005) J Biomater Sci Polymer 16:1575
34. Nishikawa M, Takakura Y, Hashida M (1996) Adv Drug Delivery Rev 21:135